Mid-Miocene cosmogenic upper limit for $^{10}Be/^{21}Ne$ burial age

Yan Ma[a]*, Weitao Wang[a], Dewen Zheng[a], Huiping Zhang[a], Jianzhang Pang[a], Ying Wu[a], Finlay M. Stuart[b] and Sheng Xu[b]

[a] *State Key Laboratory of Earthquake Dynamics, Institute of Geology, China Earthquake Administration, Beijing, 100029*

[b] *Scottish Universities Environmental Research Centre (SUERC), East Kilbride, G75 0QF, UK*

* Corresponding author.

E-mail address: mayan82634@hotmail.com

Phone number: (86) 13641123884

Present address: State Key Laboratory of Earthquake Dynamics, Institute of Geology, China Earthquake Administration, Yard No.1jia, Hua Yan Li, Chaoyang District, Beijing, 100029, China

Declarations of interest: none

Abstract

Cosmogenic nuclide burial dating provides an alternative method for sediment dating, and the combination of radionuclide ^{10}Be with noble gas isotope ^{21}Ne would theoretically extend the burial dating range up to around 15 Ma ago, which endows $^{10}Be/^{21}Ne$ pair with huge potential in middle-Miocene sediment dating. Especially in the magnetostratigraphic studies of the Cenozoic sedimentary strata, the $^{10}Be/^{21}Ne$ pair could be expected to provide absolute age marker when the well-dated volcanic ash layer or bedded mammalian fossils are absent. However, the validity and accuracy of the $^{10}Be/^{21}Ne$ burial dating when used close to its limiting middle Miocene ages has not been assessed in case study. Here, we show our dating results of the sedimentary stratum samples, which deposited at the same bedding of the Vertebrate fossils of *Platybelodon tongxinensis* that offer an independent age constraint between 12 and 15 Ma. The $^{10}Be/^{21}Ne$ analyses yielded a mean burial age of 13.25±0.33 Ma, which agrees well with the paleontological proxy, and the MSWD value of 0.66 indicates the good agreement of the apparent dispersion of six aliquots data with their individual measurement errors. In view of the extended applicable dating range of $^{10}Be/^{21}Ne$ pair, it is promising in providing absolute age marker or valuable chronological information for a variety of fields in Earth science and beyond.

Keywords: Cosmogenic burial dating; $^{10}Be/^{21}Ne$; Mid-Miocene; Sediment dating

1. Introduction

Sediments record crucial information about the erosional and sedimentary processes (e.g., Balco et al., 2013; Granger et al., 2015; Ivy-Ochs and Briner, 2014; Matmon et al., 2012), and are regarded as the key to understanding issues of how landscape evolves as well as how geomorphic processes interact with tectonic activities and/or climatic changes (e.g., Bishop, 2010; Burbank et al., 1996). However, suitable chronological methods for sediment dating on the timescales of millions of years are actually scarce. Magnetostratigraphy can afford unique

chronological sequences for the continental sediments relying on an age marker of well-dated volcanic ash layer or bedded mammalian fossils, but this independent age constraint is not always available in every sedimentary stratum (Balco and Shuster, 2009).

Cosmogenic nuclide burial dating provides an alternative method for sediment dating (Granger and Muzikar, 2001). A pair of cosmogenic nuclides produced in the same minerals but with different half-lives, or one stable isotope and one radionuclide, in principle allows the determination of burial time since the onset of sediment deposited on the basis of the time-dependent relative concentration of this pair of nuclides (Lal, 1991; Lal and Arnold, 1985). Radioactive $^{10}Be/^{26}Al$ is the most widely used pair in burial dating because both ^{10}Be and ^{26}Al are produced in quartz whose chemical composition is simple and in which the nuclide production ratio has been well established. Shorter-lived nuclide controls the upper limit of a nuclide pair when it decays to a level that cannot be measured accurately, therefore, the $^{10}Be/^{26}Al$ nuclide pair is sensitive to the decay time on the scale of few million years dependent on the half-life of ^{26}Al, which endows it with great capability to accurately date Plio-Pleistocene sediments.

The combination of radionuclide ^{10}Be with noble gas isotope ^{21}Ne would theoretically extend the applicable range of cosmogenic burial dating up to middle Miocene of around 15 Ma ago (Balco and Shuster, 2009), and additionally the stable ^{21}Ne recorded the pre-burial exposure history of sediments more directly, which is supposed to be a promising proxy for the temporal variability of the paleo-erosion rates at source basin. However, only a few study cases have employed stable ^{21}Ne in sediment burial dating (e.g., Balco and Shuster, 2009; Davis et al., 2011; Sartégou et al., 2018), and the burial ages dated by using $^{10}Be/^{21}Ne$ pair mainly distribute in Plio-Pleistocene period.

In this work, we select an ideal sampling site, where the basin-filling process has been investigated thoroughly and the definite age sequence of the sedimentary strata has been

established. Especially, an independent age constraint from Vertebrate fossils that are mixed with the sediments we collected has further restricted the depositional time of surrounding sediments within the age range of 12-15 Ma. We aim to date the sediments here by using cosmogenic $^{10}Be/^{21}Ne$ burial dating method, in order to show the improved dating range yielded by the combination of stable nuclide ^{21}Ne with radioactive nuclides, and on the other hand, to assess the accuracy of $^{10}Be/^{21}Ne$ burial dating when used close to its limiting middle Miocene ages.

2. Geological Setting

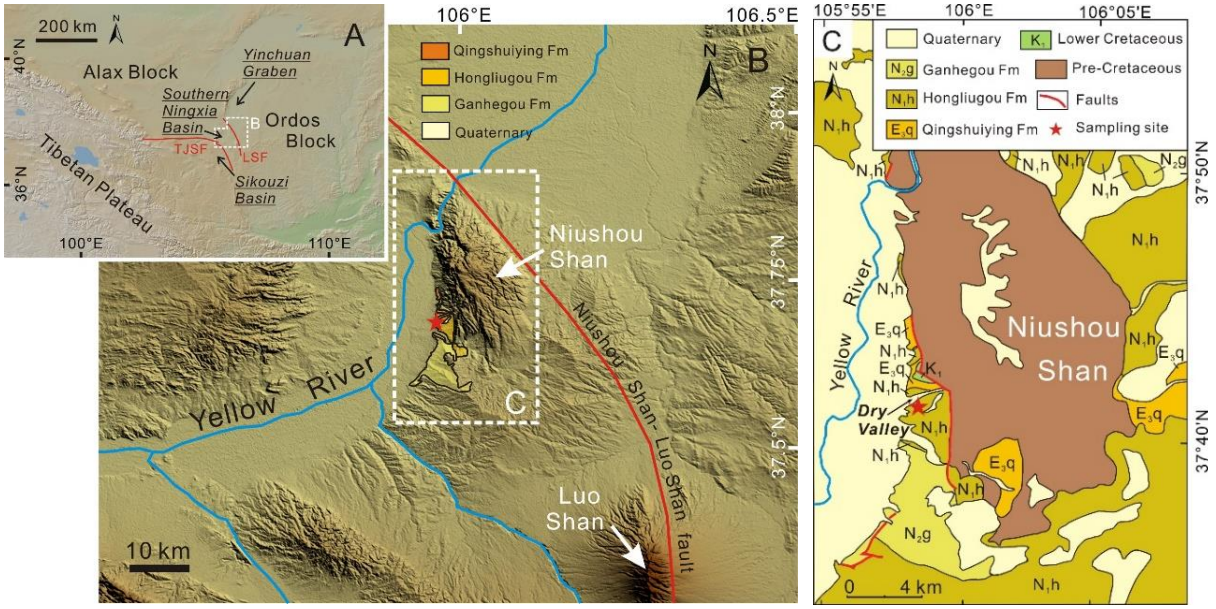

Figure 1. A: Digital elevation model (GeomapApp) image of the northeastern margin of Tibetan Plateau and its adjacent regions. White polygon outlines the region of south Ningxia basin showing in B. Abbreviations are as follows. LSF: NiuShou Shan-Luo Shan fault; TJSF: Tianjing Shan fault. B: Topographic map of the southern Ningxia Basin showing the sampling site with the red star. Strata are marked locally just surrounding the sampling site. White rectangle shows the location of C. C: Geological map surrounding the sampling site showing distributions of the Cenozoic stratigraphy.

The study area is located in the southern Ningxia Basin, NW China, where is at the tectonic junction zone of the northeastern Tibetan Plateau, Ordos block and Alax block. The southern Ningxia Basin is bound by the Niushou Shan-Luo Shan (LSF) and Tianjing Shan (TJSF) faults, and thus it is separated from the Yinchuan Graben in the northeast direction and the Sikouzi Basin in the southwest (Figs. 1 A and B). Cenozoic sediments are widely deposited in this area due to the uplift and denudation of the northeastern Tibetan Plateau during its

98 northeastward progressive growth, and the lithological units spanning the age range from ~29
99 to 0.5 Ma belong to four different formations: Sikouzi, Qingshuiying, Hongliugou, and
100 Ganhegou (Wang et al., 2011). Deformation associated with the fault movement in the
101 western foothills of the Niushou Shan had generated a syncline (Zhang et al., 2010), and
102 across the north limb of this syncline, there is a section well-exposed along a NE-SW trending
103 dry valley (Fig. 1C). The deformed bedding of Hongliugou Formation, with the bedding dip
104 of 38° NE, and the overlying horizontal young Quaternary deposits are exposed along the
105 section (Figs. 2 A and B), but the Pliocene Ganhegou Formation is absent, which indicates
106 that the deformation happened coeval with the Ganhegou Formation.
107 The Hongliugou Formation is characteristic of fluvial original sediments, and is dominated
108 by red-orange mudstone, siltstone and coarse-grain sandstone. The provenance of Hongliugou
109 Formation in this region is implied by the sedimentary facies and palaeocurrent to be the
110 Xiang Shan in the southwest area which is mainly composed of Early Palaeozoic quartzose
111 sandstones (Zhang et al., 2010). Caves are recently excavated in the Hongliugou Formation
112 by local people to search for fossils, which provide ideal sampling sites for collecting the
113 buried sediments for cosmogenic burial dating. Some mammalian fossils are found to be
114 mixed with the sediments in one cave (Fig. 2A), which is roughly 0.5 m high and 25 m deep
115 in total, and the overlying sediments are more than 25 meters from the surface straight
116 downwards to the cave location (Fig. 2B).
117 The mammalian fossils recovered in this cave include *Aceratherium* (Fig. 2C),
118 *Platybelodon* (Fig. 2D) and *Lagomeryx complicidens*, and among them, a branch of left lower
119 mandible (Left M_2-M_3, Fig. 2D) is well preserved. The M_2 has three ridges, with anterior and
120 posterior serrated crests of pretrite cusps, the size of which is 115 mm× 62.3 mm, with thick
121 cement in the molar valleys. The third lower molars M_3 are hypsodont and angusticoronate
122 crown. It belongs to the 5-ridge type, with the pretrite cusps and posttrite cusps, and the

posterior serrated crests of the pretrite cusps are developed, with thick cement filled in the valleys as well. The fifth ridge has not fully erupted, without the posttrite cusp. The configuration and structure of this branch of left lower mandible are closely matched for the *Platybelodon tongxinensis* described by Ye and Jia (1986) collected from the same locality. Therefore, the specimen mixed with the cave sediments is likely to be assigned to *Platybelodon tongxinensis*, referred to as the Dingjiaergou Fauna, with an age between 12 and 15 Ma, (Chen, 1978; Qiu and Qiu, 1995), which provides an independent age constraint on the deposition time of the sediments in this cave.

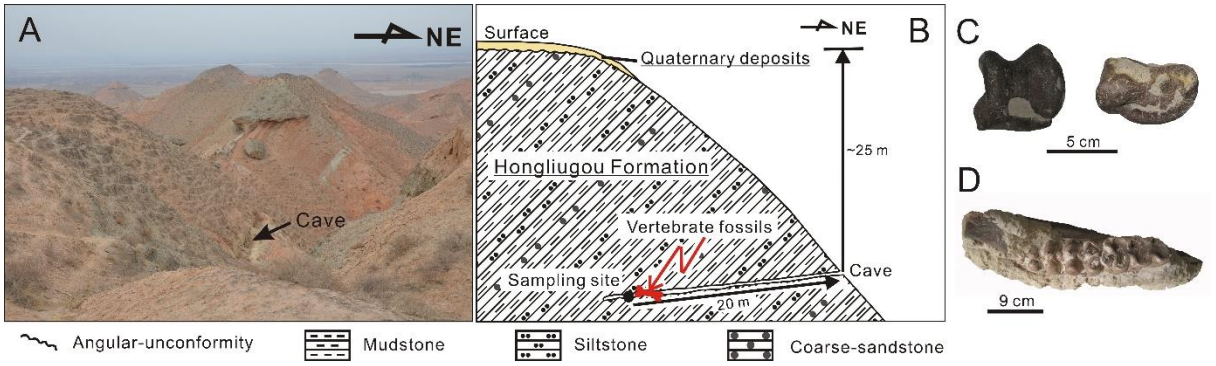

Figure 2. A: The overview of the Hongliugou Formation in the north margin of the southern Ningxia basin. The black arrow shows the cave in which we sampled. B: Profile showing the deformed Hongliugou Formation with the bedding dip of 38° NE and its angular-unconformity contact with the overlying Quaternary deposits. The sampling site is marked and the vertebrate fossils which are mixed with the sediments are shown in C and D. Vertebrate fossils that belong to *Aceratherium* (C) and *Platybelodon* (D) (locally referred to as the Dingjiaergou Fauna) are mixed with the buried sediments we sampled, suggesting an age of 12–15 Ma.

3. Material and Methods

3.1 Sample Collection

Six samples were collected at the position of 20 m inwards from the cave entrance, where are basically shielded from the cosmic-ray irradiation at present (Fig. 2B). Each aliquot is a bulk sediment collected from an area with the same length of about 20 cm for each dimension and is mainly composed of quartz-bearing sandstone, with seldom gravel clasts. Six aliquots were collected within a lateral offset of 3 m. Coarse sands were sieved out for analysis, and in order to limit the effect of spatial variability on the erosional rate at source area, only 250-500 μm grain-size fraction in the sediments was selected.

3.2 Neon and Beryllium Analyses

Sediment samples were purified to extract pure quartz basically according to the procedure reported by Kohl and Nishiizumi (1992) for ^{21}Ne and ^{10}Be analyses. Neon analyses were carried out in two laboratories for the comparison of the effect of different measurement procedure on dating results. The neon extraction was under one-step heating at 1350 °C on MAP-215 Magnetic Sector Mass Spectrometer in SUERC (Scottish Universities Environmental Research Center) and stepwise heating at four steps of 400 °C, 600 °C, 800 °C and 1350 °C on GV 5400 Noble Gas Mass Spectrometer in IGCEA (Institute of Geology, China Earthquake Administration), respectively. The neon blanks had an atmospheric composition, containing ~2×10^7 atoms of ^{20}Ne at room temperature and ~1×10^8 atoms of ^{20}Ne at high temperature. For all samples and calibrations, the abundances of masses 2, 16, 18, 19, 20, 21, 22, 40 and 44 were determined. Corrections for $^{40}Ar^{2+}$ at mass 20 and for $^{44}CO_2^{2+}$ at mass 22 were calculated from the measured mass 40 ($^{40}Ar^{+}$) and mass 44 ($^{44}CO_2^{+}$) signals by using their individual charge state ratios of $^{40}Ar^{+}/^{40}Ar^{2+}$= 4.18–4.20 and $^{44}CO_2^{+}/^{44}CO_2^{2+}$ = 104–106. The isobaric interference from $H_2{}^{18}O^{+}$ and $H^{19}F^{+}$ at mass 20 can be ignored. Detailed information about measurement procedure can be referred elsewhere (Ma et al., 2015; Vermeesch et al., 2015).

The ^{10}Be chemical separations and analyses were also carried out in two laboratories. ^{10}Be chemistry was conducted following the standard procedure (e.g., Wagner et al., 2010), and $^{10}Be/^{9}Be$ nuclide ratio in the samples and chemical procedural blanks were measured using 5 MV AMS at SUERC AMS facility and 3 MV AMS at Arizona AMS Laboratory, University of Arizona. All $^{10}Be/^{9}Be$ ratios were normalized to the NIST standard SRM-4325 with $^{10}Be/^{9}Be$ of 2.79×10^{-11} when using ^{10}Be half-life of 1.36×10^6 a (Nishiizumi et al., 2007). The chemical procedural blanks for $^{10}Be/^{9}Be$ nuclide ratio were at levels of 3.40×10^{-15} for SUERC and 3.60×10^{-15} for Arizona, which were subtracted from the measured nuclide ratios of samples as

the blank correction for the chemical procedures.

3.3 $^{10}Be/^{21}Ne$ Burial Age Calculation

For quartz samples, we use the most recently reported mean SLHL (sea level high-latitude) value of 4.15 atoms g^{-1} a^{-1} for the total ^{10}Be production rate from the Lal/Stone time dependent model (Lal, 1991; Stone, 2000) compiled by Martin et al. (2017). Based on this updated ^{10}Be production rate, cosmogenic ^{21}Ne production rate (SLHL) is calculated to be 17.5 atoms g^{-1} a^{-1} by using a $^{21}Ne/^{10}Be$ production ratio of 4.23 defined in Kober et al. (2011). The rates of production by neutron spallation are scaled with elevation and latitude by using the scaling method of Stone (2000). Attenuation length for neutron flux in the sediments of density 2.6 g cm^{-3} is adopted the value of 160 g cm^{-2} (Gosse and Phillips, 2001).

The production rate by muon reactions of ^{10}Be is determined following the model described by Granger and Smith (2000). For ^{21}Ne, however, the correlation of muon-induced production rate with depth has not yet been studied clearly, so in this work, we have followed the approximation that the muon-induced $^{21}Ne/^{10}Be$ production ratio is constant with depth Balco and Shuster (2009) used. The muon-induced nuclide production rates are just scaled for elevation using an atmospheric pressure at the sampling site of 870 g cm^{-2} and an atmospheric attenuation length of 240 g cm^{-2} (Rossi, 1948). Due to the latitudinal variation in muon flux is sufficiently small at moderate latitudes, latitude dependence of production rates by muon could be ignored (Allkofer and Jokisch, 1973).

Burial ages "t_b," are calculated assuming sediments being dated were derived from a steadily eroding process at provenance, without taking the muogenic nuclide production during the eroding process into account, therefore, cosmogenic nuclide concentrations measured in samples "$N_{i,m}$," are (Granger and Muzikar, 2001):

$$N_{i,m} = P_{s,i}/[\lambda_i + \rho_s \cdot E/\Lambda_n] \cdot \exp(-t_b \cdot \lambda_i) + N_{i,pb} \quad (1)$$

where i= 10 and 21 for ^{10}Be and ^{21}Ne, respectively; t_b is the burial time from sediments were

deposited; E is the steady erosion rate, which is referred as the paleo-erosion rate at provenance; $N_{i,pb}$ is nuclide accumulation after sample deposited; $P_{s,i}$ is the average basin-wide nuclide production rate at provenance, which is calculated by scaling the SLHL rate to the assumed elevation and latitude of the catchment basin at provenance. Here, considering the provenance of the sediments originated from the mountain ranges at the northeastern margin of Tibetan Plateau, we roughly constrain the average altitude of the watershed in the level of 2000 m, and neglect the latitude variation; λ_i is the radioactive decay constant, and for ^{21}Ne, $\lambda_{21}= 0$; ρ_s is rock density at the source area where the sediments originated from, and we use the typical value of 2.6 g cm^{-3} in this work; and Λ_n is the attenuation length for neutron flux.

Combination of ^{10}Be and ^{21}Ne could theoretically yield the burial age and the paleo-erosion rate at source basin provided the post-burial nuclide concentration can be independently estimated. When taking no account of the post-burial nuclide concentrations, a ^{21}Ne/^{10}Be burial age could be calculated based on Eq. 1 as following:

$$t_b = -(1/\lambda_{10}) \cdot \ln[(N_{10,m}/N_{21,m}) \times (P_{s,21}/P_{s,10}) + (N_{10,m}/P_{s,10}) \times \lambda_{10}] \quad (2)$$

Symbols are the same as those defined in Eq. 1. The resultant age from Eq. 2 is referred as simple burial age here.

The post-burial nuclide concentrations in samples from a steadily accumulating landscape could be calculated following the approach reported by Hetzel et al. (2004):

$$N_{i,pb} = \frac{P_{i,n} \cdot \exp(-\alpha \cdot t_b \cdot \rho/\Lambda_n)}{\lambda_i - \rho \cdot \alpha/\Lambda_n} \cdot \{1 - \exp[-(\lambda_i - \rho \cdot \alpha/\Lambda_n) \cdot t_b]\}$$

$$+ \sum_{j=1}^{3} \{\frac{P_{i,\mu-j} \cdot \exp(-\alpha \cdot t_b \cdot \rho/\Lambda_{\mu-j})}{\lambda_i - \rho \cdot \alpha/\Lambda_{\mu-j}} \cdot \{1 - \exp[-(\lambda_i - \rho \cdot \alpha/\Lambda_{\mu-j}) \cdot t_b]\}\} \quad (3)$$

where the first term is for nuclide concentration by neutron spallation, with $P_{i,n}$ indicating the surface production rates at sampling location. For this work, the cave location is 37.7001°N and 105.9768°E, with the elevation of 1266 m; the rest three terms are referring to

muon-induced nuclide concentrations, in which $P_{i,\mu\text{-}j}$ is the production rate by muon reaction at the sampling location and $\Lambda_{\mu\text{-}j}$ is the attenuation length for muon flux (Granger and Smith, 2000, and references therein); ρ is sediment density of Hongliugou Formation and was determined to 2.6 g cm^{-3}; α is the sediment accumulation rate in basin, and the value is given by 10 cm ka^{-1} based on the magnetostratigraphy study in the adjacent basin of Sikouzi (Wang et al., 2011), which represents the combined effects of sedimentation and denudation occurred during the sediment deposition. Other symbols are the same as those defined before.

The post-burial nuclide concentration in sample is firstly roughly estimated according to Eq. 3 by using the simple burial age. Then, correcting the measured ^{10}Be and ^{21}Ne concentrations in Eq. 1 for their respective post-burial production and combining the two nuclides, the paleo-erosion rate (E) is determined and the burial age (t_b) is recalculated. Iterate the above process until the resultant burial age converges on a solution.

4. Results

Considering the long depositional time would result extremely low ^{10}Be concentrations in samples that were close to the detection limit of AMS measurement, we have used twice the amount for routine samples to keep the amount of ^{10}Be maintaining at the order of 10^5 atoms, in order to minimize measurement errors for ^{10}Be. The measurement results of ^{10}Be and ^{21}Ne analyses for six aliquots are summarized in Tabs. 1-2.

As expected, the ^{10}Be/^{9}Be isotopic ratio is only several times higher than the blank level even twice the amount for routine sample was used, and the uncertainties of resultant ^{10}Be concentration is high. As for neon analysis, all data points of neon isotope ratios from either the one-step heating or the four-step heating basically lie on the spallation line within the measurement uncertainties (Niedermann et al., 1993) in the neon three-isotope diagram illustrated in Fig. 3, indicating no significant non-cosmogenic ^{21}Ne released before 1350°C. The resultant concentrations of cosmogenic ^{21}Ne in six aliquots are listed in Tab. 3.

247

Table 1. Data for ^{10}Be analysis with 1σ uncertainties

Sample	Mass of quartz (g)	Mass of Be carrier (mg)	^{10}Be/^{9}Be* (× 10^{-13})	error (1σ)	^{10}Be† (×10^{5} atom)	error (1σ)	[^{10}Be]§ (×10^{3} atom g^{-1})	error (1σ)	rel.# (%)
SUERC AMS									
Blank CFG1602	N.D.**	0.2332	0.0340	0.0073	N.D.	N.D.	N.D.	N.D.	N.D.
HLV-03	41.391	0.2241	0.1576	0.0133	1.17	0.206	2.83	0.498	17.6
HLV-04	64.021	0.2244	0.2561	0.0123	2.50	0.195	3.91	0.304	7.78
HLV-05	55.343	0.2256	0.2104	0.0170	1.90	0.253	3.44	0.456	13.3
HLV-06	32.612	0.2249	0.1518	0.0113	1.10	0.184	3.37	0.564	16.7
HLV-07	47.904	0.2254	0.2168	0.0122	1.99	0.195	4.15	0.408	9.83
Arizona AMS									
Blank HZB32	N.D.	0.3134	0.0360	0.0148	N.D.	N.D.	N.D.	N.D.	N.D.
HLV-10	52.032	0.3157	0.1289	0.0250	2.45	0.474	3.40	1.057	31.1

Note: ^{10}Be analyses carried out in two laboratories, with samples HLV-03—HLV-07 in SUERC AMS facility (SUERC AMS), and HLV-10 in Arizona AMS Laboratory (Arizona AMS).

*The measurements are normalized to ^{10}Be primary standard NIST SRM4325 with ^{10}Be/^{9}Be ratio of 2.79×10^{-11} when using ^{10}Be half-life of 1.36 Ma (Nishiizumi et al., 2007).

†The total amount of ^{10}Be atom in the samples, having been corrected for blanks.

§The blank-corrected ^{10}Be concentrations are calculated from the measured ^{10}Be/^{9}Be ratios of the samples and the respective blank.

#The relative error of ^{10}Be concentration.

**N.D.= no data.

248

249

Table 2. Data for neon isotope measurements with 1σ uncertainties

Sample ID	*Weight* (g)	*T*(°C)	[^{20}Ne] (×10^{9} at g^{-1})	error (1σ)	[^{21}Ne] (×10^{6} at g^{-1})	error (1σ)	^{21}Ne/^{20}Ne* (×10^{-3})	error (1σ)	^{22}Ne/^{20}Ne* (×10^{-3})	error (1σ)	[^{21}Ne]$_c$† (×10^{6} at g^{-1})	error (1σ)
SUERC												
HLV-03	0.435	1350	34.35	0.026	117.2	0.82	3.37	0.033	102.5	0.36	14.38	1.20
HLV-04	0.396	1350	23.70	0.024	82.89	0.87	3.46	0.043	102.7	0.35	11.92	1.08
HLV-05	0.419	1350	26.29	0.054	93.64	1.15	3.52	0.050	102.8	0.53	14.91	1.38
HLV-06	0.412	1350	25.84	0.045	90.82	1.26	3.47	0.054	102.6	0.45	13.45	1.44
HLV-07	0.423	1350	21.15	0.010	78.24	0.99	3.66	0.055	103.0	0.69	14.89	1.25
IGCEA												
HLV-10	1.005	400	2.19	0.065	8.64	0.81	3.94	0.369	102.8	1.00	2.15	0.21
		600	8.83	0.042	31.74	1.71	3.59	0.194	103.2	0.72	5.60	0.36
		800	11.86	0.040	38.19	1.17	3.22	0.100	102.3	0.80	3.08	0.14
		1350	1.92	0.089	8.64	0.54	4.50	0.286	104.1	1.06	2.95	0.21
										Total§	13.78	0.49

Note: Data set of neon measurements carried out in two laboratories, with samples HLV-03—HLV-07 in Isotope Geoscience Laboratory of SUERC, and HLV-10 in Neotectonics and Geochronology Laboratory of IGCEA.

*The ratios of ^{21}Ne/^{20}Ne and ^{22}Ne/^{20}Ne are normalized by the ratios of air calibration. The uncertainties in air calibration with the values of 0.7% for ^{21}Ne/^{20}Ne and 0.4% for ^{22}Ne/^{20}Ne are propagated into the sample data.

†Cosmogenic ^{21}Ne concentration in the samples, calculated as the sum of the excesses ^{21}Ne. Excess ^{21}Ne is calculated without applying blank corrections and assuming an atmospheric origin of all the measured ^{20}Ne according to the equation of $[^{21}Ne]_{ex} = [^{21}Ne]_m \times (R_m - R_a)/R_m$, in which R_m is the measured ^{21}Ne/^{20}Ne-ratio, and R_a is the atmospheric ^{21}Ne/^{20}Ne-ratio, with the value of 0.002959 (Eberhardt et al., 1965). The uncertainties in the air calibrations are included in the reported uncertainties.

§The cosmogenic ^{21}Ne concentration calculated using the ^{21}Ne excesses in four heating steps of 400, 600, 800 and 1350 °C.

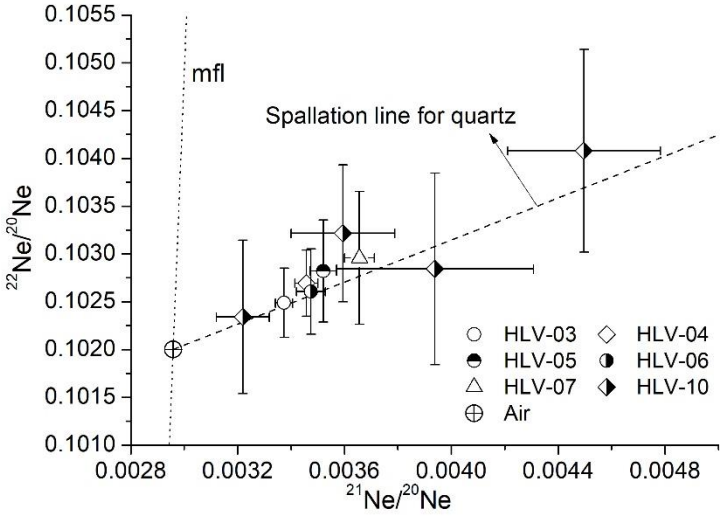

Figure 3. Ne three-isotope diagram for buried sediment samples. For samples HLV-03—HLV-07, the data of Ne isotope ratios are from one-step heating extraction at 1350°C, and for sample HLV-10, showing the data from stepwise heating extractions at 400°C, 600°C, 800°C, and 1350°C. Mixtures of atmospheric and cosmogenic neon plot on the spallation line, whose slope has been experimentally determined to be 1.120±0.021 for quartz (Niedermann et al., 1993). The dotted line mfl means the mass fractionation line. Error bars represent 1σ uncertainties.

The $^{10}Be/^{21}Ne$ burial ages of six aliquots and the corresponding paleo-erosion rates at source area are listed in Tab. 3. The average age of six aliquots is calculated to be 13.25±0.33 Ma (Fig. 4), with high measurement precision of 2.46%. The accuracy of the measured burial age has been verified by the mammal fossils of *Platybelodon tongxinensis* that suggests the time period during 12-15 Ma. The MSWD (Mean Square of the Weighted Deviates) value is calculated to be 0.66, which indicates the good agreement of the apparent dispersion of six aliquots data with their individual measurement errors.

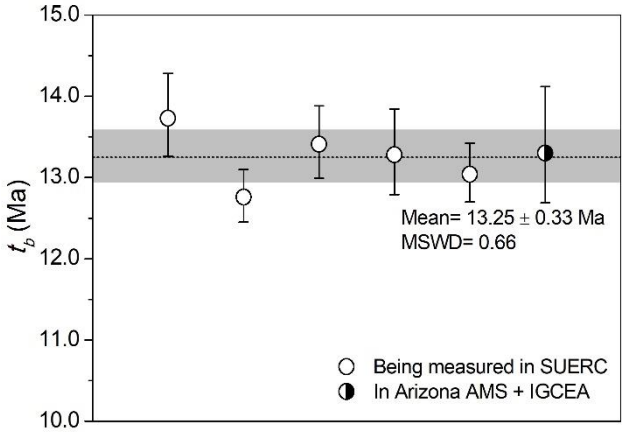

Figure 4. Overview of the measured burial ages of six aliquots and the analytical uncertainties. The dotted line and gray band show the average burial age of this set of data and the 1σ uncertainty of 13.25±0.33 Ma.

267 Table 3. Burial ages and paleo-erosion rates from ^{10}Be and ^{21}Ne in sediments

Sample ID	Nuclide	Measured concentration (atom g^{-1} SiO_2)	Post-burial nuclide concentration* (atom g^{-1} SiO_2)						t_b† (Ma)	*Paleo-erosion rate* E§ (cm ka^{-1})
			Neutron	Negative muon-1	Negative muon-2	Fast muon	Total	N_{pb}/N_m (%)		
HLV-03	^{10}Be	2.83±0.50 ×10^3	57.57	3.66	2.98	6.27	70.48	2.5	13.73 (+0.55/-0.47)	0.32±0.03
	^{21}Ne	1.44±0.12 ×10^7	2.68×10^5	1.67×10^4	1.31×10^4	2.66×10^4	3.24×10^5	2.3		
HLV-04	^{10}Be	3.91±0.30 ×10^3	94.41	6.00	4.89	10.28	115.58	3.0	12.76 (+0.34/-0.31)	0.39±0.04
	^{21}Ne	1.19±0.11 ×10^7	2.68×10^5	1.67×10^4	1.31×10^4	2.66×10^4	3.24×10^5	2.7		
HLV-05	^{10}Be	3.44±0.46 ×10^3	67.77	4.31	3.51	7.38	82.97	2.4	13.41 (+0.47/-0.42)	0.31±0.03
	^{21}Ne	1.49±0.14 ×10^7	2.68×10^5	1.67×10^4	1.31×10^4	2.66×10^4	3.24×10^5	2.2		
HLV-06	^{10}Be	3.37±0.56 ×10^3	72.42	4.61	3.75	7.88	88.66	2.6	13.28 (+0.56/-0.49)	0.34±0.04
	^{21}Ne	1.35±0.14 ×10^7	2.68×10^5	1.67×10^4	1.31×10^4	2.66×10^4	3.24×10^5	2.4		
HLV-07	^{10}Be	4.15±0.41 ×10^3	81.85	5.21	4.24	8.91	100.20	2.4	13.04 (+0.38/-0.34)	0.31±0.03
	^{21}Ne	1.49±0.13 ×10^7	2.68×10^5	1.67×10^4	1.31×10^4	2.66×10^4	3.24×10^5	2.2		
HLV-10	^{10}Be	3.40±1.06 ×10^3	71.68	4.56	3.71	7.80	87.76	2.6	13.30 (+0.82/-0.61)	0.33±0.01
	^{21}Ne	1.38±0.05 ×10^7	2.68×10^5	1.67×10^4	1.31×10^4	2.66×10^4	3.24×10^5	2.4		

Note: Cave location is 37.7001°N and 105.9768°E, and the site elevation at the cave entrance is 1266 m. The elevation of the catchment basin at sediment provenance is adopted the value of 2000 m, taking no account of the latitude variation. For quartz samples, the total production rates at sea level and high latitude (SLHL) of 4.15 atoms g^{-1} a^{-1} for ^{10}Be (Martin et al., 2017) and 17.5 atoms g^{-1} a^{-1} for ^{21}Ne (Kober et al., 2011; Martin et al., 2017) are used. Production rate of neutron spallation is scaled for elevation and latitude using Stone (2000) scaling method with a factor of 2.54. Rate of muon-induced production is just scaled for elevation using an atmospheric attenuation length of 240 g cm^{-2} (Rossi, 1948) and atmospheric pressure at the sampling site is 870 g cm^{-2}, therefore the resultant scaling factor for muon production rate over SLHL is $e^{[(1013-870)/240]}$= 1.81. The radioactive decay constant of ^{10}Be is used λ_{10}= 5.10×10^{-7} a^{-1} (Nishiizumi et al., 2007), in order to be consistent with the value we used when choosing the isotopic ratio of ^{10}Be AMS standard.

*The individual contribution of four reaction mechanisms, neutron spallation, two terms of slow negative muons capture, and fast muons reaction, is listed separately, and the total value means the sum of the above four data.

†Burial ages are calculated taking the post-burial nuclide production into account. The uncertainties of burial ages are just the propagation of analytical errors of ^{10}Be and ^{21}Ne concentrations, which do not include the uncertainties of decay constant of ^{10}Be and production rates.

§Erosion rates in source area, the muon-induced nuclide production during eroding process is not included in calculation. The uncertainties only originated from the analytical uncertainties of nuclide concentrations, but errors of post-burial nuclide concentrations, production rates and the decay constant of ^{10}Be have not been included.

We have plotted the data on the $^{21}Ne/^{10}Be$ concentration ratio *v.s.* ^{10}Be concentration diagram (Fig. 5). After correcting the post-burial nuclide production, the data points of all aliquots drop in a region confined by the burial age ranging from 12 to 14 Ma and the paleo-erosion rate spanning from 0.3 to 0.5 cm ka^{-1}, consistent with the calculated results by iterated method.

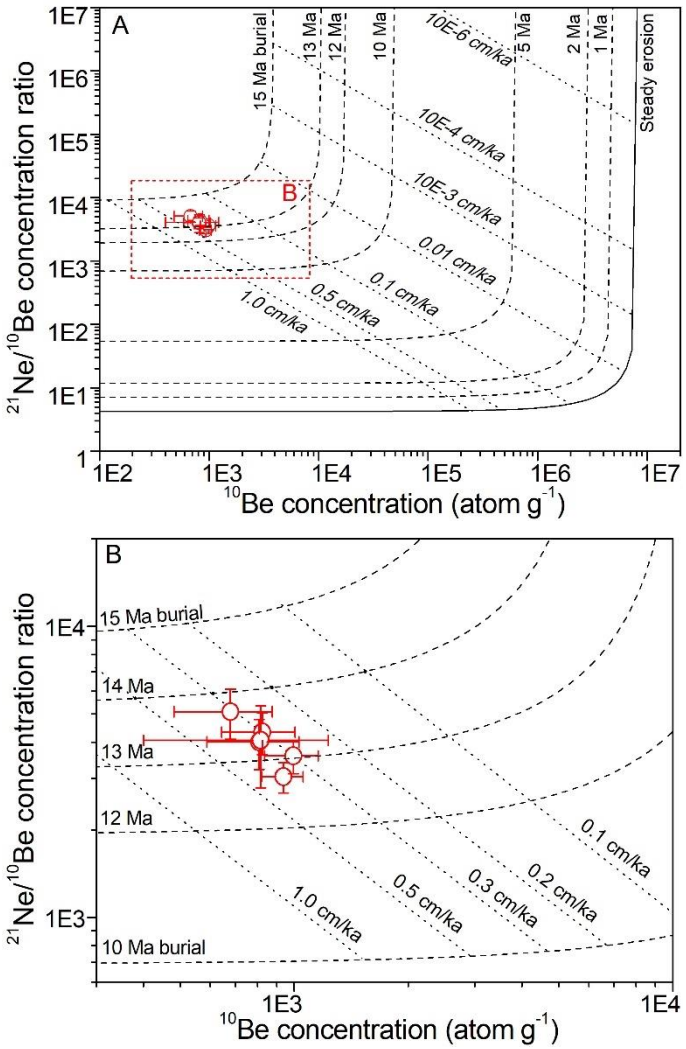

Figure 5. Burial dating plot showing the $^{21}Ne/^{10}Be$ ratio and the ^{10}Be concentration of six aliquots of sediments, collected from the Hongliugou Formation in the southern Ningxia basin, with a density of 2.6 g cm^{-3} on the logarithmic axes, and the nuclide concentrations are normalized to the nuclide production rate at SLHL. A: Solid line represents the $^{21}Ne/^{10}Be$ ratio evolution under steady-state erosion. The pre-exposure period erosion rates are shown in the range of 10^{-6} to 1.0 cm ka^{-1} in italic, and the set of parallel dotted lines indicate the change of $^{21}Ne/^{10}Be$ ratio under different erosion rates when samples were buried and completely shielding from the cosmic radiation. The dash lines show the isolines of burial ages in the range of 1 to 15 Ma, calculated using the steady erosion model. The data of six aliquots corrected for post-burial production and normalized to SLHL are showed as the red circles, and error bars represent 1σ uncertainties. The red rectangle showing the array in the vicinity of the data of six aliquots is enlarged in B. B: Enlarged $^{21}Ne/^{10}Be$ burial plot for these six aliquots.

The post-burial nuclide production involving spallation and muon reactions has been taken

into account in this study in order to accurately determine the burial ages, and the post-burial nuclide concentrations induced by different reactions are listed in Tab. 3 as well. As expected, the post-burial nuclide production just makes a minor contribution to the total nuclide concentrations measured in samples for both ^{10}Be and ^{21}Ne, which are negligible. On the other hand, in post-burial nuclide concentration, the majority contribution is still from neutron spallation, more than 80% of the total amounts. Although the fast muon-induced production is insignificant at surface, due to its long attenuation length, the fast muon reaction nearly makes an equal contribution as the negative muon does to the total nuclide production at sufficient depth.

5. Discussion

Under some situations, the validity and accuracy of the burial dating depends strongly on the geological models used to describe the histories sediments had experienced. As a result, we interpret the influence of the geological assumptions involved in this case on the burial dating results.

5.1 Uncertainties derived from the pre-exposure histories

Firstly, the nuclide concentration ratio before burial would be lower than their production rate ratio. For the low erosion rate at provenance of this work, the assumption that the initial nuclide concentration ratio between ^{10}Be and ^{21}Ne is equal to their production ratio is not valid because the precondition of $\rho_s \cdot E/\Lambda_n >> \lambda_{10}$ does not hold true (Granger and Muzikar, 2001). As a result, the radioactive decay of ^{10}Be during the long pre-burial history could not be neglected, otherwise, it would lead to the overestimate of the burial age. Moreover, the nuclide production rates of the watershed at provenance have been estimated by using a basin-average altitude of 2000 m, but actually, the average elevation of the source basin is probably higher than what we assumed. To take the uncertainty from this assumption into account, we have considered the influence from a variation of 500 m attached to the

312 catchment average elevation on the calculated burial age as well as the paleo-erosion rate. In
313 the case of sample HLV-03, for example, the paleo-erosion rate was then estimated to be
314 0.46±0.04 cm ka^{-1} and the corresponding burial age was determined to be 13.79(+0.56/-0.48)
315 Ma. It is revealed that the adopted average elevation of source catchment basin has no
316 significant influence on the burial age determination, just a 0.4% increase for HLV-03, while
317 results in non-negligible influence on the paleo-erosion rate estimation, which increases from
318 0.32±0.03 to 0.46±0.04 cm ka^{-1} with the provenance elevation increasing from 2000 to 2500
319 m.

320 On the other hand, for this work, the muogenic nuclide production in the pre-exposure
321 history is not taken into account due to its contribution is insignificant compared to the
322 neutron spallation production at surface and shallow depth (Granger and Smith, 2000). If the
323 contribution of muogenic nuclide production is included in the calculation following the
324 approach described by Lupker et al. (2012), the burial dating result, by taking the sample
325 HLV-03 as example again, has shown a negligible change, with the decrease less than 1%,
326 while, the paleo-erosion rate yields a significant increase which is up to 13%. Therefore, it
327 seems that the burial age determination is less affected by the assumptions adopted in the
328 pre-exposure period, in contrast, the calculated paleo-erosion rate would change significantly
329 under different conditions associated to the sediment provenance.

330 *5.2 Influence of the depositional process on the burial age calculation*

331 We have assumed a steady accumulation model of sediments in the basin at a rate of 10 cm
332 ka^{-1}, based on the magnetostratigraphic constraint of a section located in the adjacent basin of
333 Sikouzi (Wang et al., 2011). The apparent sedimentary rate is reported to slightly increase to
334 ~24 cm ka^{-1} during the period of 5-2 Ma ago and sedimentary hiatus has been proven to occur
335 (Wang et al., 2011). However, because that the post-burial nuclide concentration is just
336 sensitive to the accumulation rate of the first few meters of sediment immediately overlying

samples (Balco et al., 2005), and samples would be buried deeper than 5000 g cm^{-2} after no more than one million years in the case of 10 cm ka^{-1} of accumulation rate, the rate change of sediment accumulation beyond this period would not affect the post-burial nuclide production and the accuracy of burial dating.

As for the geological context of samples after deposition, the deformation of the Hongliugou Formation caused the change on burial depth of samples. Whereas, this tectonic deformation is considered to occur during or later than Pliocene indicated by the absence of the Pliocene deposit of Ganhegou Formation. Samples had been deeply buried at that time and their nuclide inventories were on longer sensitive to buried depth. Therefore, the resultant burial ages in this case are supposed not to be affected by the complicated geological context sediments had experienced.

However, there are still some significant error sources on the calculated burial ages than those described above which derive from breaking down the assumption of single episodic burial for sediments. For example, if the quartz has been reworked from old deposits, the calculated burial age will overestimate the true depositional age, which lead to gross mistake in the interpretation of the age data. However, it is difficult to recognize multiple episodes of burial histories by using $^{10}Be/^{21}Ne$ nuclide pair. The way to identify reworked samples by constructing an isochron has proved to be effective for $^{10}Be/^{26}Al$ burial dating (Balco and Rovey, 2008), but there is no successful attempt on the isochron $^{10}Be/^{21}Ne$ burial dating till now.

6. Conclusions

We have selected an ideal sampling site with an independent age constraint of 12-15 Ma for a preliminary proof of the Mid-Miocene upper limit of $^{10}Be/^{21}Ne$ burial dating method. The resultant $^{10}Be/^{21}Ne$ burial age of 13.25±0.33 Ma agrees well with the paleontological proxy, and the MSWD value of 0.66 indicates the good agreement of the apparent dispersion of six

aliquots data with their individual measurement errors. The uncertainties of the burial ages mainly derive from errors of nuclide measurements, but uncertainties in decay constants and production rates have propagated into an intrinsic uncertainty in resultant ages which could not be reduced. Geological models adopted in this case have been proven not to propagate significant uncertainties into burial ages. The extended burial dating range of $^{10}Be/^{21}Ne$ pair endows it with huge potential in the applications of middle Miocene sediment dating, which makes it a promising technique to provide absolute age marker or valuable chronological information for a variety of fields in geoscience and even beyond.

Acknowledgements

This work was jointly supported by Grants-in-Aid from the basic scientific research fund, Institute of Geology, China Earthquake Administration (Grant No. IGCEA1504), the State Key Laboratory of Earthquake Dynamics (Grant No. LED2017A05), and the basic scientific research fund, Institute of Geology, China Earthquake Administration (Grant No. IGCEA1417). The authors express their sincere thanks to Prof. Zhaoqun Zhang in Institute of Vertebrate Paleontology and Paleoanthropology, Chinese Academy of Sciences for his expertise with the mammalian fossil identification, to Dr. Fei Han at the Institute of Geology, China Earthquake Administration for his constructive suggestion on burial age determination.

References

Allkofer, O., and Jokisch, H., 1973. A survey on the recent measurements of the absolute vertical cosmic-ray muon flux at sea level. Il Nuovo Cimento A (1965-1970), v. 15, no. 3, pp. 371-389.

Balco, G., and Rovey, C. W., 2008. An isochron method for cosmogenic-nuclide dating of buried soils and sediments. American Journal of Science, v. 308, no. 10, pp. 1083-1114.

Balco, G., and Shuster, D. L., 2009. ^{26}Al–^{10}Be–^{21}Ne burial dating. Earth Planet Sci Lett, v.

286, pp. 570–575.

Balco, G., Soreghan, G. S., Sweet, D. E., Marra, K. R., and Bierman, P. R., 2013. Cosmogenic-nuclide burial ages for Pleistocene sedimentary fill in Unaweep Canyon, Colorado, USA. Quat Geochronol, v. 18, pp. 149-157.

Balco, G., Stone, J. O., and Mason, J. A., 2005. Numerical ages for Plio-Pleistocene glacial sediment sequences by $^{26}Al/^{10}Be$ dating of quartz in buried paleosols. Earth Planet Sci Lett, v. 232, no. 1, pp. 179-191.

Bishop, P., 2010. Long-term landscape evolution: linking tectonics and surface processes. Earth Surf Process Landf, v. 32, no. 3, pp. 329-365.

Burbank, D. W., Leland, J., Fielding, E., Anderson, R. S., Brozovic, N., Reid, M. R., and Duncan, C., 1996. Bedrock incision, rock uplift and threshold hillslopes in the northwestern Himalayas. Nature, v. 379, no. 6565, pp. 505–510.

Chen, G., 1978. Some mastodont from Miocene of Ningxia. Vert PalAsiat, v. 16, no. 2, pp. 103-110 (in Chinese).

Davis, M., Matmon, A., Fink, D., Ron, H., and Niedermann, S., 2011. Dating Pliocene Lacustrine Sediments In The Central Jordan Valley, Israel—Implications For Cosmogenic Burial Dating. Earth Planet Sci Lett, v. 305, pp. 317–327.

Eberhardt, P., Eugster, O., and Marti, K., 1965. Notizen: A Redetermination of the Isotopic Composition of Atmospheric Neon. Z Naturforsch A, v. 20, no. 4, pp. 623-624.

Gosse, J. C., and Phillips, F. M., 2001. Terrestrial in situ cosmogenic nuclides: theory and application. Quat Sci Rev, v. 20, no. 14, pp. 1475-1560.

Granger, D. E., Gibbon, R. J., Kuman, K., Clarke, R. J., Bruxelles, L., and Caffee, M. W., 2015. New cosmogenic burial ages for Sterkfontein Member 2 Australopithecus and Member 5 Oldowan. Nature, v. 522, no. 7554, pp. 85-88.

Granger, D. E., and Muzikar, P. F., 2001. Dating sediment burial with in situ-produced

412 cosmogenic nuclides: theory, techniques, and limitations. Earth Planet Sci Lett, v. 188,
413 no. 1, pp. 269–281.
414 Granger, D. E., and Smith, A. L., 2000. Dating buried sediments using radioactive decay and
415 muogenic production of ^{26}Al and ^{10}Be. Nucl Instrum Methods Phys Res B, v. 172, no.
416 1, pp. 822-826.
417 Hetzel, R., Tao, M. X., Stokes, S., Niedermann, S., Ivy-Ochs, S., Gao, B., Strecker, M. R.,
418 and Kubik, P. W., 2004. Late Pleistocene/Holocene slip rate of the Zhangye thrust
419 (Qilian Shan, China) and implications for the active growth of the northeastern
420 Tibetan Plateau. Tectonics, v. 23, pp. TC6006.
421 Ivy-Ochs, S., and Briner, J. P., 2014. Dating disappearing Ice with cosmogenic nuclides.
422 Elements, v. 10, no. 5, pp. 351-356.
423 Kober, F., Alfimov, V., Ivy-Ochs, S., Kubik, P. W., and Wieler, R., 2011. The cosmogenic
424 ^{21}Ne production rate in quartz evaluated on a large set of existing ^{21}Ne–^{10}Be data.
425 Earth Planet Sci Lett, v. 302, no. 1–2, pp. 163-171.
426 Kohl, C., and Nishiizumi, K., 1992. Chemical isolation of quartz for measurement of
427 in-situ-produced cosmogenic nuclides. Geochim Cosmochim Ac, v. 56, no. 9, pp.
428 3583-3587.
429 Lal, D., 1991. Cosmic ray labeling of erosion surfaces: in situ nuclide production rates and
430 erosion models. Earth Planet Sci Lett, v. 104, no. 2, pp. 424-439.
431 Lal, D., and Arnold, J. R., 1985. Tracing quartz through the environment. Proc Indian Acad
432 Sci Earth Planet Sci, v. 94, no. 1, pp. 1-5.
433 Lupker, M., Blard, P. H., Lavé, J., France-Lanord, C., Leanni, L., Puchol, N., Charreau, J.,
434 and Bourlès, D., 2012. ^{10}Be-derived Himalayan denudation rates and sediment budgets
435 in the Ganga basin. Earth Planet Sci Lett, v. 333–334, no. 6, pp. 146-156.
436 Ma, Y., Wu, Y., Li, D., and Zheng, D., 2015. Analytical procedure of neon measurements on

GV 5400 noble gas mass spectrometer and its evaluation by quartz standard CREU-1. Int J Mass Spectrom, v. 380, no. 2, pp. 26-33.

Martin, L. C. P., Blard, P. H., Balco, G., Lavé, J., Delunel, R., Lifton, N., and Laurent, V., 2017. The CREp program and the ICE-D production rate calibration database: A fully parameterizable and updated online tool to compute cosmic-ray exposure ages. Quat Geochronol, v. 38, pp. 25-49.

Matmon, A., Stock, G. M., Granger, D. E., and Howard, K. A., 2012. Dating of Pliocene Colorado River sediments: Implications for cosmogenic burial dating and the evolution of the lower Colorado River. Geol Soc Am Bull, v. 124, no. 3-4, pp. 626-640.

Niedermann, S., Graf, T., and Marti, K., 1993. Mass spectrometric identification of cosmic-ray-produced neon in terrestrial rocks with multiple neon components. Earth Planet Sci Lett, v. 118, no. 1, pp. 65-73.

Nishiizumi, K., Imamura, M., Caffee, M. W., Southon, J. R., Finkel, R. C., and Mcaninch, J., 2007. Absolute calibration of Be-10 AMS standards. Nucl Instrum Methods Phys Res B, v. 258, pp. 403-413.

Qiu, Z., and Qiu, Z., 1995. Chronological sequence and subdivision of Chinese Neogene mammalian faunas. Palaeogeogr Palaeoclimatol Palaeoecol, v. 116, no. 1–2, pp. 41-70.

Rossi, B., 1948. Interpretation of cosmic-ray phenomena. Rev Mod Phys, v. 20, no. 3, pp. 537.

Sartégou, A., Bourlès, D. L., Blard, P. H., Braucher, R., Tibari, B., Zimmermann, L., Leanni, L., Aumaître, G., and Keddadouche, K., 2018. Deciphering landscape evolution with karstic networks: A Pyrenean case study. Quat Geochronol, v. 43, pp. 12-29.

Stone, J., 2000. Air pressure and cosmogenic isotope production. J Geophys Res, v. 105, no.

462 B10, pp. 23753-23759.
463 Vermeesch, P., Balco, G., Blard, P.-H., Dunai, T. J., Kober, F., Niedermann, S., Shuster, D. L.,
464 Strasky, S., Stuart, F. M., and Wieler, R., 2015. Interlaboratory comparison of
465 cosmogenic ^{21}Ne in quartz. Quat Geochronol, v. 26, pp. 20-28.
466 Wagner, T., Fabel, D., Fiebig, M., Häuselmann, P., Sahy, D., Xu, S., and Stüwe, K., 2010.
467 Young uplift in the non-glaciated parts of the Eastern Alps. Earth Planet Sci Lett, v.
468 295, no. 1–2, pp. 159-169.
469 Wang, W. T., Zhang, P. Z., Kirby, E., Wang, L. H., Zhang, G. L., Zheng, D. W., and Chai, C.
470 Z., 2011. A revised chronology for Tertiary sedimentation in the Sikouzi basin:
471 Implications for the tectonic evolution of the northeastern corner of the Tibetan
472 Plateau. Tectonophysics, v. 505, no. 1, pp. 100-114.
473 Ye, J., and Jia, H., 1986. Platybelodon (Proboscidea, Mammalia) from the middle Miocene of
474 Tongxin, Ningxia. Vert PalAsiat, v. 24, no. 2, pp. 61-92 (in Chinese).
475 Zhang, J., Dickson, C., and Cheng, H. Y., 2010. Sedimentary characteristics of Cenozoic
476 strata in central-southern Ningxia, NW China: Implications for the evolution of the
477 NE Qinghai-Tibetan Plateau. J Asian Earth Sci, v. 39, no. 6, pp. 740–759.
478
479